# Dynamical Reconstruction of Upper-Ocean Conditions in the Last Glacial Maximum Atlantic

HOLLY DAIL AND CARL WUNSCH

*Massachusetts Institute of Technology, Cambridge, Massachusetts*

(Manuscript received 10 April 2013, in final form 31 August 2013)

ABSTRACT

Proxies indicate that the Last Glacial Maximum (LGM) Atlantic Ocean was marked by increased meridional and zonal near sea surface temperature gradients relative to today. Using a least squares fit of a full general circulation and sea ice model to upper-ocean proxy data with specified error estimates, a seasonally varying reconstruction is sought of the Atlantic Ocean state that is consistent with both the known dynamics and the data. With reasonable uncertainty assumptions for the observations and the adjustable (control) variables, a consistent LGM ocean state is found, one not radically different from the modern one. Inferred changes include a strengthening of the easterly and westerly winds, leading to strengthened subtropical and subpolar gyres, and increased upwelling favorable winds off the coast of Africa, leading to particularly cold SSTs in those regions.

## 1. Introduction

As compared to preindustrial conditions, the Last Glacial Maximum (LGM; 19 000–23 000 years ago) climate was marked by a lowering of atmospheric $CO_2$ concentration by about 90 ppm (Barnola et al. 1987), a lowering of sea level by about 125 m (Lambeck and Chappell 2001), and a large expansion of ice sheets, which covered much of northern North America and northern Europe at the LGM (Peltier 2004). The consequences for the ocean circulation of this radically different climatology are of intense interest. Recently, relatively complete compilations of ocean near sea surface temperature (NSST) proxies from that period have become available, ones that carry potentially useful information about the circulation. The adjective ''near'' is used to distinguish these temperatures, which are traditionally based on calibrations for the top 10 m of the ocean (and which depend on organisms that may live as deep as 200–400 m). In the meteorological literature, SST is at the surface itself and can be a skin temperature, not reflecting the temperature below.

Proxy data show clear evidence for increased zonal and meridional NSST gradients in the Atlantic Ocean at the LGM, among other changes (MARGO Project Members 2009). However, existing coupled model simulations have not been able to reproduce these patterns (Kageyama et al. 2006; Otto-Bliesner et al. 2009). These mismatches indicate problems exist in the models and/or in the data, but the sources of the model data differences remain obscure. To further complicate matters, different proxy estimates sometimes strongly disagree among themselves (De Vernal et al. 2006; Leduc et al. 2010), as do the coupled model simulations (Kageyama et al. 2006; Otto-Bliesner et al. 2007).

This study seeks a reconciliation of model and data discrepancies through a ''dynamical reconstruction,'' defined here to be an estimate of the seasonally varying ocean state that is consistent both with known ocean physics and with available proxy observations—within their uncertainties. In the literature on the modern circulation, the methodology is known as ''state estimation.'' As carried out here, a least squares fit of a full ocean general circulation model (GCM) is made to LGM NSST proxy observations. After the adjustment of uncertain model parameters, the model is run forward in a free mode, so that the equations governing the estimated state are known exactly.

A number of methods are available for fitting time-evolving numerical models to observed data. Here, the

*Corresponding author address:* H. Dail, Department of Earth and Planetary Sciences, Harvard University, 20 Oxford St., Cambridge, MA 02138.
E-mail: holly.dail@gmail.com

DOI: 10.1175/JCLI-D-13-00211.1

method of Lagrange multipliers [sometimes known to oceanographers as the adjoint method and to meteorologists as four-dimensional variational data assimilation (4DVAR)] is used. Although these methods have been used extensively for the modern ocean (e.g., Stammer et al. 2002; Wunsch and Heimbach 2007, 2013), application to paleo-reconstruction problems has been only tangential. For example, Winguth et al. (1999) used the Lagrange multiplier method with cadmium/calcium and carbon isotopic ratio ($\delta^{13}$C) LGM proxy observations and a simplified general circulation model in which adjustable parameters were restricted to surface salinity.

In other paleostudies, so-called static inverse methods were applied under the assumption that the ocean can be described by steady-state equations. Gebbie and Huybers (2006) reconstructed the LGM meridional circulation rates at 30°S through a combination of oxygen isotopic ratios ($\delta^{18}$O) and a geostrophic inverse model. Static inverse methods have also been applied to reconstruct deep-ocean conditions throughout the Atlantic Ocean. These have relied on benthic $\delta^{13}$C and $\delta^{18}$O measurements (LeGrand and Wunsch 1995; Marchal and Curry 2008) or on ratios of protactinium to thorium isotopes (Pa-231/Th-230; Burke et al. 2011). The generic problem of determining paleoceanographic circulations was reviewed by Huybers and Wunsch (2010), with much of the focus on the need for methods that determine rates of flow, as opposed to water mass volumes. Although rate-determining tracers do exist (notably $^{14}$C), almost all information about the intensity of the modern ocean circulation comes from a combination of knowledge of the externally prescribed curl of the wind stress and the internally determined geostrophic hydrostatic balance (Huybers and Wunsch 2010). One seeks estimation methods for the paleocirculation that incorporate these features.

Although no uniquely best approach seems to exist, in any estimation problem the greatest insights come from the use of a model that, given available data, has a relatively well-sampled domain and an appropriate level of complexity. Here, the focus is on the Atlantic Ocean, which (of the world oceans) has by far the highest density of LGM proxy data, and on upper-ocean conditions, which are closely linked to sea ice distributions and atmospheric forcing and have comparatively short adjustment times to changes. In contrast, adjustment times of the abyssal ocean to changes in surface conditions, oceanic or meteorological, are extremely long. A discussion of deeper flows, determined from a combination of abyssal proxies, the physics of the present model, and a consideration of extended adjustment times, will be published elsewhere.

Proxies exist for many paleoocean characteristics [see Henderson (2002) and Hillaire-Marcel and De Vernal (2007) for broad reviews, Lynch-Stieglitz (2003) for a discussion of deep-ocean proxies, and Waelbroeck et al. (2005) for a thorough discussion of uncertainties and biases in the use of a specific proxy (the oxygen isotopic ratios of planktonic foraminifera), many of which apply more generally]. The dynamical reconstruction approach used here can be applied to a wide variety of proxy types. As compared to other potential proxies, NSST data for the LGM are significantly more numerous, have been reconstructed with a diversity of approaches, and have better defined uncertainties, making these data an appropriate first target for dynamical reconstruction.

This study can be thought of as an exploratory one—in which a first attempt is made to apply the full numerical machinery of modern time-dependent state estimation and a complete GCM with the LGM oceanic state. The following key questions are addressed: 1) Are Atlantic Ocean LGM NSST patterns as inferred from proxy data physically reasonable? Is it possible to find a circulation state that is consistent with these data and with known dynamics? 2) How large are the atmospheric changes implied by the data? 3) What are reasonable uncertainty estimates on proxy data, and how sensitive is the inferred climate to these estimates?

## 2. Background

### *a. The LGM NSST data*

Relatively extensive compilations of LGM NSST proxies have been produced by Climate: Long-Range Investigation, Mapping, and Prediction (CLIMAP; CLIMAP Project Members 1976); Glacial Atlantic Ocean Mapping Project (GLAMAP; Sarnthein et al. 2003); and Multiproxy Approach for the Reconstruction of the Glacial Ocean Surface (MARGO; Kucera et al. 2005a). The most recent and comprehensive of these efforts, MARGO, developed global compilations based on diverse proxy approaches and dedicated substantial effort to providing quantitative uncertainties on each proxy record (MARGO Project Members 2009). Site-specific proxy reconstructions with accompanying uncertainty estimates were produced for individual cores, as well as a synthesis $5° \times 5°$ gridded estimate with its own uncertainty estimates. In this paper, only the site-specific data are considered.

Four MARGO compilations have significant coverage in the Atlantic Ocean, and all of them are used here: foraminiferal (Kucera et al. 2005b; Hayes et al. 2005) and dinoflagellate cyst (De Vernal et al. 2005) assemblages,

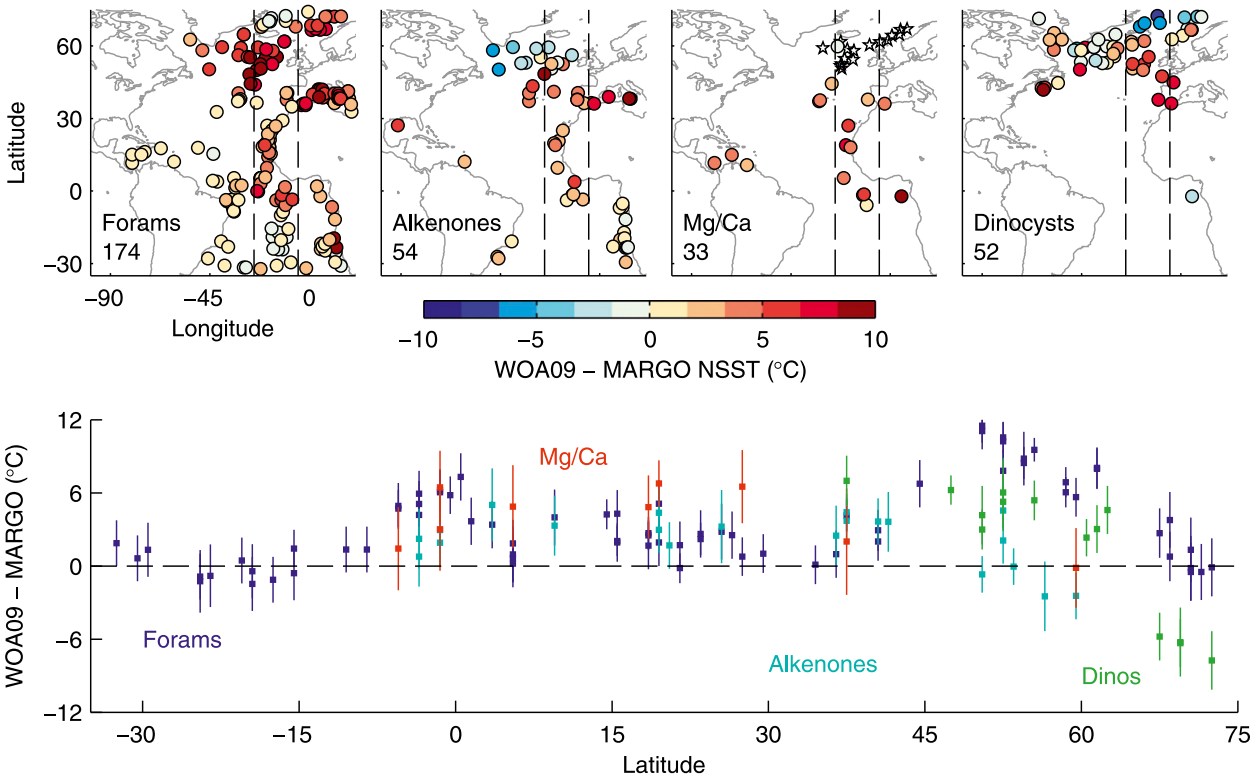


FIG. 1. Difference between annual-mean NSSTs from the *2009 World Ocean Atlas* (*WOA09*) and MARGO LGM estimates. (top) Maps for each proxy type are overlaid with the number of applicable records (lower left corner of each map); the longitude band of 25°–5°W is marked with dashed lines. (bottom) Data from this band are plotted against latitude, with vertical lines marking $\pm\sigma$ ranges with $\sigma$ given by the MARGO-defined uncertainties of MARGO Project Members (2009). Note that MARGO reported most high-latitude Mg/Ca estimates as summer mean only; these are marked with stars in the map and are not shown in the lower plot.

foraminiferal Mg/Ca (Barker et al. 2005), and the alkenone $U_{37}^{K'}$ index (Rosell-Melé et al. 2004). Assumptions of seasonality in MARGO vary by proxy: annual-, winter-, and summer-mean NSST reconstructions were published for the foraminiferal and dinocyst assemblage proxies; only annual-mean reconstructions were published for the alkenone records; and annual-mean (summer mean) reconstructions were published for low-latitude (high latitude) Atlantic Mg/Ca records.

Despite the relatively comprehensive nature of MARGO, the distribution of observations (Fig. 1, top) shows a lack of data in some regions (e.g., in the Gulf Stream path) and uneven data coverage elsewhere (e.g., dinocyst data are available in high-latitude locations only). Examining modern to LGM temperature changes against latitude (Fig. 1) makes evident that, especially in the high latitudes, the proxies are sometimes inconsistent with each other in the magnitude, and even in the sign, of modern to LGM NSST change (see also De Vernal et al. 2006; Kageyama et al. 2006). For example, north of 45°N the foraminiferal assemblage–based reconstruction shows LGM temperatures much colder than modern ones, while the dinocyst-based reconstruction shows LGM temperatures warmer than today's.

Providing uncertainty estimates for proxy-based observations is challenging: many assumptions must be made in the conversion from a proxy record to an estimate of a climate property such as temperature, and these assumptions can introduce substantial biases and other errors (see, e.g., Telford et al. 2013). MARGO Project Members (2009) assigned uncertainty estimates to each MARGO NSST estimate using a formula that combined quantitative estimates of calibration error with qualitative evaluations of data quality associated with, for example, the number of samples used to make the reconstructed NSST estimate and the dating uncertainty. These final uncertainties were labeled "semi-quantitative" by MARGO Project Members (2009) and were defined only within an unknown factor (where unity was suggested as a reasonable first estimate). With that factor of unity, MARGO-defined standard errors range from 0.8° to 4.9°C with a mean of 2.3°C. As seen in Fig. 1, these estimates of the uncertainties on the reconstructions

obtained with each proxy separately are insufficient to account for the disagreements between proxies, particularly north of about 40°N.

### b. *Existing model results and comparisons to the data*

Although a wide variety of models have been applied individually to the LGM, we focus here on the Paleoclimate Modelling Intercomparison Project (PMIP), an extensive, long-running effort to create and compare coupled model estimates of the LGM climate (Braconnot et al. 2012). Of the three phases of PMIP, PMIP2 (Braconnot et al. 2007) is the most recent for which the model results have been widely published (PMIP3 results are only now becoming available). In PMIP2, coupled ocean–atmosphere and ocean–atmosphere–vegetation models were run under a standard set of LGM boundary conditions including ice sheets and topography as reconstructed in "ICE-5G" (Peltier 2004), greenhouse gas concentrations, and orbital forcing parameters.

Kageyama et al. (2006) compared PMIP models and site-specific MARGO data in the North Atlantic between about 25° and 85°N. Significant inter-model and model-data discrepancies were found for estimated LGM meridional NSST gradients. Otto-Bliesner et al. (2009) also used the site-specific MARGO data but focused on the tropics between 15°S and 15°N. Although estimates of the annual-mean tropical cooling were consistent between PMIP2 models and MARGO, regional and seasonal patterns of change were different. The MARGO reconstructions indicated stronger cooling in northern summer than in northern winter and stronger cooling in the eastern equatorial Atlantic than in the western. In contrast, the PMIP2 models produced relatively uniform LGM cooling in the tropics, both spatially and across the seasons. Hargreaves et al. (2011) compared PMIP2 models with the $5° \times 5°$ gridded MARGO NSST estimates, which are more highly smoothed and have different uncertainty estimates than the site-specific estimates. Hargreaves et al. treated the PMIP2 models as an ensemble and found that the ensemble spread was neither too broad nor too narrow to represent the gridded MARGO estimate.

A quantitative summary of the fit of each PMIP2 model's estimated NSSTs to those of the site-specific MARGO data can be made as follows. Following the notation of Wunsch (2006), any evolving model $\mathbf{L}$ of a physical system can be written in discrete time as

$$\mathbf{x}(t+\Delta t) = \mathbf{L}\{\mathbf{x}(t), \mathbf{q}(t), \mathbf{u}(t)\}, \quad 0 \le t \le t_f, \tag{1}$$

where $t_f = M\Delta t$ where M is the number of time steps; $\mathbf{x}(t)$ is the model state at time $t$, discrete at intervals $\Delta t$, and includes prognostic or dependent variables computed by a model, such as the temperature or salinity; $\mathbf{q}(t)$ denotes known forcings, sources, sinks, internal model parameters, and boundary and initial conditions; and $\mathbf{u}(t)$ is any such elements that are regarded as uncertain, including model errors, but also uncertainties in model parameters and initial and boundary conditions. Elements $\mathbf{u}(t)$ are adjustable control variables and are always equal to zero in forward models such as the PMIP2 models.

Useful observations $\mathbf{y}(t)$ taken at time $t$ are all functions of the actual physical state $\mathbf{x}(t)$ and are nearly always a linear combination of state vector elements:

$$\mathbf{y}(t) = \mathbf{E}(t)\mathbf{x}(t) + \mathbf{n}(t), \quad 1 \le t \le t_f, \tag{2}$$

where $\mathbf{n}(t)$ is the noise in the observations. The misfit of a model to data can be computed as the normalized quadratic model data differences:

$$J_{\text{data}} = \frac{1}{NM} \sum_{m=1}^{M} [\mathbf{y}(t) - \mathbf{E}(t)\mathbf{x}(t)]^{\mathrm{T}} [\mathbf{R}(t)]^{-1} [\mathbf{y}(t) - \mathbf{E}(t)\mathbf{x}(t)], \tag{3}$$

where $t = m\Delta t$, $M$ is the number of model time steps included in the comparison, $N$ is the number of observations, and $\mathbf{R}$ is a matrix of observational error covariances. To simplify, and in the absence of adequate knowledge of actual covariances, observation noise is assumed to be uncorrelated so that $\mathbf{R}$ is a diagonal, with diagonal elements given by the square of the MARGO uncertainties of MARGO Project Members (2009) used with a factor of 1.

Using this formulation, a $J_{\text{data}}$ of order 1 indicates the model is within the average uncertainty of the data—that the fit is nominally acceptable. As shown in Fig. 2, the PMIP2 models are inconsistent with the site-specific MARGO data in the Atlantic, given assumed uncertainties. Although this result disagrees with that of Hargreaves et al. (2011), important differences between the methods (consideration of the ensemble as a whole versus consideration of each model separately) and the target datasets (gridded versus site-specific MARGO) complicate comparison of the results.

## 3. Dynamical reconstruction approach

An estimate of ocean circulation at the LGM is sought that is consistent with both ocean dynamics and the MARGO NSST data, given estimated uncertainties in the data. Only a summary of our approach is provided here [see Heimbach et al. (2005), Wunsch and Heimbach (2007), and Dail (2012) for more extended descriptions].

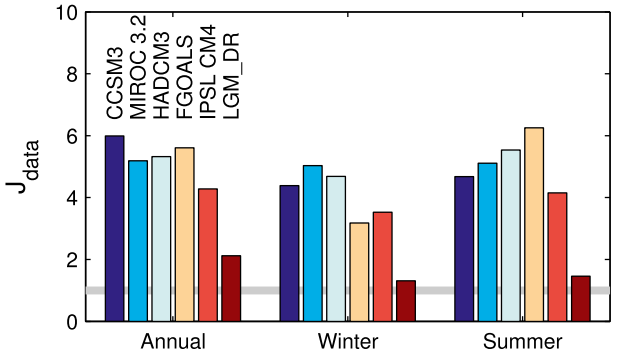


FIG. 2. Model data misfit $J_{\text{data}}$ [Eq. (3)] between six models and all MARGO proxy records, evaluated in the Atlantic Ocean from 35°S to 75°N. The first five models are PMIP2 coupled model simulations of the LGM run under standard LGM boundary conditions [see Braconnot et al. (2007) for details], and LGM_DR is the current study. To compute $J_{\text{data}}$ for this figure, the published uncertainties of MARGO Project Members (2009) are used for all models, including LGM_DR. A $J_{\text{data}}$ of order 1 (marked with a gray line) is indicative of consistency of the model with the data and their uncertainty assumptions.

TABLE 1. Model parameters used throughout this study.

| Parameter name | Value |
|---|---|
| Lateral diffusivity | $1 \times 10^{2}\,\mathrm{m^2\,s^{-1}}$ |
| Vertical diffusivity | $1 \times 10^{-5}\,\mathrm{m^2\,s^{-1}}$ |
| Laplacian lateral viscosity | $1 \times 10^{4}\,\mathrm{m^2\,s^{-1}}$ |
| Laplacian vertical viscosity | $1 \times 10^{-3}\,\mathrm{m^2\,s^{-1}}$ |
| GM thickness diffusivity | $1 \times 10^{3}\,\mathrm{m^2\,s^{-1}}$ |
| Quadratic bottom drag | $2 \times 10^{-3}$ |

The dynamical reconstruction is defined as determining a state $\mathbf{x}(t)$ for $1 \le t \le t_f$, and controls $\mathbf{u}(t)$ for $0 \le t \le t_f - \Delta t$ exactly satisfying Eqs. (1) and (2). The problem is one of constrained optimization, in which one seeks to minimize a cost function composed of the normalized quadratic model data differences and the control variable adjustments $\mathbf{u}(t)$:

$$J = \sum_{m=1}^{M} [\mathbf{y}(t) - \mathbf{E}(t)\mathbf{x}(t)]^{\mathrm{T}} [\mathbf{R}(t)]^{-1} [\mathbf{y}(t) - \mathbf{E}(t)\mathbf{x}(t)] + \sum_{m=0}^{M-1} [\mathbf{u}(t)]^{\mathrm{T}} [\mathbf{Q}(t)]^{-1} \mathbf{u}(t), \quad (4)$$

where $t = m\Delta t$ and $\mathbf{Q}$ is a matrix of error covariances on control variables $\mathbf{u}(t)$. A weighted least squares minimization of Eq. (4) subject to Eq. (1) is sought. Vectors of Lagrange multipliers $\boldsymbol{\mu}(t)$ are used to ''adjoin'' the model equations to produce a new cost function:

$$J' = J - 2 \sum_{m=1}^{M} [\boldsymbol{\mu}(t)]^{\mathrm{T}} [\mathbf{x}(t) - \mathbf{L}\{\mathbf{x}(t - \Delta t), \mathbf{q}(t - \Delta t), \mathbf{u}(t - \Delta t)\}], \quad (5)$$

where $J$ is given by Eq. (4). Stationary values of $J'$ are then sought; the resulting solution is equivalent to the one that emerges from taking the vector derivatives of $J'$ with respect to all of $\tilde{\mathbf{x}}(t)$, $\mathbf{u}(t)$, and $\boldsymbol{\mu}(t)$, setting them to zero, and solving the resulting ''normal equations.''

Although conceptually simple, this least squares problem is technically difficult to solve in practice. A GCM, as is used here, is encapsulated in hundreds of thousands of lines of computer code and is nonlinear. Given the high dimensionality of the problem, many standard numerical solution techniques are intractable. For the method of Lagrange multipliers, $J'$ must be differentiated, which in turn requires that the GCM itself can be differentiated. GCMs, including the one used in this paper, are represented not by analytical expressions but by computer codes undergoing constant modification. Software tools have been developed that (semi)automatically generate another computer code for the adjoint (dual) model (Giering and Kaminski 1998; Heimbach et al. 2005), and it is these automatic differentiation (AD) methods that render the method practical here. The solution is obtained not by explicit solution of the normal equations but by an iterative search using $\boldsymbol{\mu}(t)$.

The Massachusetts Institute of Technology (MIT) GCM (MIT GCM) is an evolved version of that described by Marshall et al. (1997) and Adcroft et al. (2004) and is used to simulate ocean circulation under hydrostatic, Boussinesq, and linear implicit free-surface assumptions; Table 1 summarizes the model parameters. A third-order advection scheme with direct space–time treatment is used, and vertical diffusive fluxes are treated implicitly. Horizontal resolution is $1° \times 1°$ latitude–longitude in an Arakawa C grid (Arakawa and Lamb 1977) in a domain extending from 40°S to 80°N. In the vertical 50 levels are used, ranging in thickness from 10 m at the surface to 450 m at depth. At the resolution used here, some dynamical processes are poorly resolved; in particular, one expects upwelling regions to be overly broad and weak, and the dynamics of the equatorial region are poorly represented. Experience with the modern ocean suggests that the model is very close to thermal wind balance below 100 m, and that, in requiring this balance in the interior, the not fully resolved

boundary currents are forced to have appropriate volume and property transports.

Eddy-induced mixing of properties along isentropes is parameterized with the GM/Redi scheme (Redi 1982; Gent and McWilliams 1990), and near-surface vertical mixing is parameterized with a turbulent kinetic energy–based model (Gaspar et al. 1990). Side (bottom) boundary conditions are free slip (no slip), and the ''C-D'' scheme is used to reduce the grid-scale noise that is commonly a problem on latitude–longitude grids (Adcroft et al. 1999). Asynchronous time stepping is used to accelerate computation; Dail (2012) showed that this approach has a minor impact on model solutions. Air–sea boundary conditions are prescribed for air temperature, zonal and meridional wind speeds, relative humidity, precipitation, runoff, and incoming shortwave and longwave radiation. Bulk formulae are used to compute wind stress, evaporation, and outgoing longwave radiation following Large and Yeager (2004). A full viscous plastic dynamic–thermodynamic sea ice model is used (Losch et al. 2010); this model is fully coupled to the ocean circulation model and uses the same grid and atmospheric forcing.

The influence of adjustable inflow and outflow through the 40°S southern boundary of the model is represented by prescribing temperatures, salinities, and horizontal velocities at all longitudes and all depths of the section across 40°S. Interior ocean properties are gradually relaxed to prescribed boundary condition properties over a sponge layer that extends from 36° to 40°S; the relaxation time scale is linearly increased from ½ day at 40°S to 10 days at 36°S. This approach reduces artificial discontinuities and wave generation associated with the boundary.

Although important sea ice and seawater transports to and from the Arctic exist at 80°N in the modern Atlantic, the details of the exchange are uncertain. Published ocean state estimates, such as the Ocean Comprehensible Atlas (OCCA; Forget 2010) and Estimating the Circulation and Climate of the Ocean, version 3 (ECCO V3; Wunsch et al. 2009), do not include the Arctic and thus cannot be used as a reasonable first estimate of conditions at 80°N. The LGM exchange is particularly uncertain as the Bering Strait was closed at that time. Given the current lack of data, the simplest choice is made here and a wall is imposed at 80°N. This choice is likely to lead to overly warm and salty conditions in the northern portion of the domain because the normal exchange of warm salty Atlantic waters with cold, fresh Arctic waters is prevented; inflow from the Arctic to the Atlantic in the East Greenland Current is also a source of sea ice to the northern North Atlantic, so the imposition of a wall may interfere with the model's capacity to produce enough sea ice in this region. Because of the relatively unphysical nature of the model configuration near the northern and southern boundaries, all simulations are run on the 40°S–80°N domain, but all analyses and figures are restricted to 35°S–75°N, with the assumption that there interior data will be determinant.

Control variables in this study, the elements of $\mathbf{u}(t)$, are the ocean temperature and salinity at every grid point that the model is initialized from (initial conditions); the temperature, salinity, and horizontal velocities at every depth and longitude of the 40°S open boundary; and atmospheric forcing variables applied at every latitude and longitude of the surface ocean (the wind speeds, air temperature, incoming shortwave radiation, specific humidity, and precipitation). Southern boundary and atmospheric forcing controls are permitted to have monthly variability but are assumed to repeat annually. Because the focus here is on the large-scale ocean circulation, atmospheric adjustments that are spatially smooth and large scale are preferred. This preference is enforced through the application of a smoothing operator to the control vector as described by Weaver and Courtier (2001). As written in Eq. (4), adjustments to control variables are penalized relative to assumed uncertainties, which are taken to be spatially uniform and constant in time.

Several important assumptions are made in the search for a dynamically consistent state of the LGM Atlantic. First, in the absence of evidence to the contrary, atmospheric and oceanic states that are relatively close to modern ones are preferred over states radically different from today's. Second, it is assumed that the LGM Atlantic can be adequately represented as seasonally varying but otherwise fixed in time. The seasonal cycle dominates the climate system and its presence is essential at and near the ocean surface. Although variability on interannual-to-millennial time scales must have occurred within the LGM, MARGO data points likely represent integrated conditions over thousands of years. Third, it is assumed that the modeled upper-ocean state responds rapidly to changes in atmospheric forcing, sufficiently so that the upper-ocean state is reasonably well defined by the second half of the 10-yr simulations. Therefore, all simulations reported in this paper are 10 yr in length and the cost function $J'$ is evaluated over the last 5 yr of each simulation; all results are reported for year 8, which falls at the midpoint of the 5-yr period included in the cost function. This comparatively short integration time is not fundamental and could be extended with additional effort (Dail 2012).

## 4. Testing with the modern circulation

The modern circulation, which is much better observed and understood than that of the LGM, is used to test model adequacy and to understand the shortcomings.

TABLE 2. Prior uncertainties for atmospheric controls in modern and LGM dynamical reconstructions.

| Variable | Mod_DR | LGM_DR |
|---|---|---|
| Shortwave radiation ($W\,m^{-2}$) | 10 | 20 |
| 2-m air temperature (°C) | 1 | 4 |
| 10-m zonal wind speed ($m\,s^{-1}$) | 1 | 2 |
| 10-m meridional wind speed ($m\,s^{-1}$) | 1 | 2 |
| 2-m specific humidity ($kg\,kg^{-1}$) | $1 \times 10^{-3}$ | $2 \times 10^{-3}$ |
| Precipitation ($m\,s^{-1}$) | $2 \times 10^{-8}$ | $4 \times 10^{-8}$ |

An existing modern state estimate made using the same Lagrange multiplier machinery, OCCA (Forget 2010), for the time-varying global ocean state over 2004–06, is used as a reference. This estimate is preferred over climatology as a target because it is demonstrably consistent with ocean physics and with a wide variety of observations and because the atlas includes self-consistent, gridded estimates of temperature, salinity, and velocity. A mean annual cycle of ocean conditions is obtained by computing monthly-mean OCCA conditions across 2004–06; this estimate will be referred to as OCCA hereafter, recognizing that it is an average of the full version. We ask a simple question: can the dominant ocean properties of OCCA be reproduced with a reduced model and using the dynamical reconstruction approach? OCCA came from a direct fit to observations and the present test becomes instead a fit to the time-averaged OCCA. Note that the model configuration used here is a simplified, and regionally restricted, version of the one used in OCCA and is not expected to fully mimic the OCCA ocean state.

Bathymetry, grid resolution, and vertical levels in our model configuration are identical to those of Forget (2010). The 2006 National Centers for Environmental Prediction–National Center for Atmospheric Research (NCEP–NCAR) reanalysis product (an updated version of Kalnay et al. 1996) is used to drive the model. Daily mean atmospheric forcing is used, under the assumption that the diurnal cycle is not of first-order importance in setting the large-scale properties of the Atlantic Ocean. The model is started from OCCA temperatures and salinities, and OCCA properties are used to prescribe southern boundary conditions. To search for solutions close to the actual modern climate state, relatively small uncertainty assumptions are used for the control variables (see Table 2). The model is constrained by OCCA temperatures and salinities at all grid points, with assumed uncertainties on OCCA properties given by the hydrographic uncertainties of Forget and Wunsch (2007). Among many differences between OCCA and the present setup, the use here of a much longer estimate length and of a repeating seasonal cycle make reproducing OCCA properties a challenge.

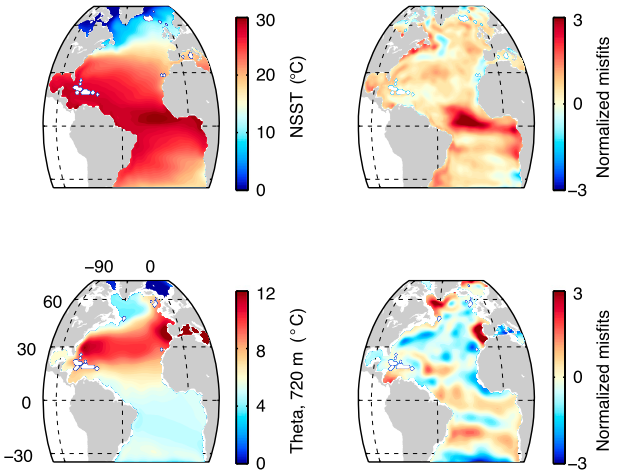


FIG. 3. (left) Near-surface and 720-m annual-mean temperatures in Mod_DR. (right) Normalized misfits to OCCA NSST and 720-m temperatures (Mod_DR − OCCA)/$\sigma$, where $\sigma$ is defined by Forget and Wunsch (2007). Normalized misfits of order 1 indicate consistency of Mod_DR and OCCA, but some smaller and larger values, as seen here, are expected for a $\chi^2$ variable. The fit to OCCA appears acceptable.

An initial ocean circulation estimate is required before proceeding with improving the fit of the model to OCCA; this prior estimate was generated by running the forward model with the above-defined prior estimates of atmospheric forcing and initial and boundary conditions (i.e., control variables are zero). The estimate was then iteratively improved. After 20 iterations, total cost $J$ [Eq. (4)] was reduced by 82%. While the prior estimate had a poor fit to OCCA [$J_{\text{data}} = 5.0$; see Eq. (3)], after 21 iterations the estimated ocean state was consistent ($J_{\text{data}} = 0.9$). This fit to OCCA is sufficient to proceed, and the iteration 21 estimate, which will hereafter be referred to as Mod_DR [for modern dynamical reconstruction (DR)], is briefly analyzed with a focus on the differences between the estimates [see Dail (2012) for more extensive analyses].

Compared to OCCA, Mod_DR is consistently warmer in the near-surface ocean (see Fig. 3). Because mixed layer physics are parameterized here with Gaspar et al. (1990), while OCCA used that of Large et al. (1994), some change is expected. Near-surface equatorial conditions are not well reproduced. This region is likely particularly sensitive to the choice of internal model parameters, which differ in the two models. Other models also have difficulty in this region: PMIP2 preindustrial simulations are consistently 2°–4°C warmer than the modern in the eastern equatorial Atlantic (Otto-Bliesner et al. 2009). Finally, at 720 m, large-scale biases are not present, but some difficulty in reproducing water mass properties is apparent in the Mediterranean outflow region and in the

Labrador Sea. These are both regions of water mass formation, a process that is highly sensitive to model numerics that vary between OCCA and the current approach. The OCCA estimate is itself not "truth" and, overall, our inference is that modern upper-ocean temperatures and salinities are relatively well represented by the dynamical reconstruction approach.

## 5. Application to Last Glacial Maximum

All MARGO data that fall within the domain of 35°S–75°N are used to constrain the estimate (see Fig. 1 for locations). The inconsistencies of the MARGO data in the high latitudes make evident that either the different proxy types are not recording the same climatic conditions, or a factor of 1 in the uncertainties is an underestimation. Accordingly, a factor of 2 is applied for all dinoflagellate cyst data and on all alkenone data north of 40°N; using larger uncertainties has the effect of downweighting these data in the dynamical reconstruction. Alkenone data are downweighted because 1) these data are thought to record warm-season temperatures in colder regions (Schneider et al. 2010), as opposed to the annual mean, as reported in MARGO; and 2) the sensitivity of the calibration is low at cold temperatures (Conte et al. 2006). Dinocyst data are downweighted based on the arguments of Dale (2001), who note a variety of serious concerns regarding reconstructions of past ocean conditions with dinocysts: in cold regions, dinoflagellates survive the winter in a dormant cyst phase and thus are unlikely to record characteristics of wintertime conditions; dinocysts are small and easily transported over long distances, so that many of the cysts in sediment samples may have originated in distant ocean regions, and many of the species used for reconstruction have broad tolerances for temperature, limiting their utility in reconstructing this environmental parameter.

LGM bathymetry is given by a smoothed version of the ICE-5G LGM reconstruction, which incorporates an LGM sea level lowering of 125 m (Peltier 2004). In keeping with the assumption that climates close to the modern are preferred over radically different ones, relatively small uncertainty assumptions are assigned to prior control variables (see the LGM_DR column of Table 2).

### *a. Prior estimate of LGM conditions*

A major difficulty in determining the LGM ocean circulation lies with the great uncertainty in existing understanding of surface atmospheric conditions at the LGM. Few proxy records of the LGM atmospheric state exist, and substantial PMIP2 model data misfits (Fig. 2) and disagreements among the models reflect that uncertainty. As part of a cautious approach to this problem, we seek LGM estimates in which the meteorology differs as little as possible from the modern world, which thus serves as the initial estimate of atmospheric forcing. In a data rich estimation problem, arbitrarily large deviations from the initial estimate can theoretically be deduced from the model data misfit. In practice, even the modern ocean database is inadequate to remove all uncertainty from the estimates of the open-ocean meteorological surface fields of recent decades.

A long-term mean of modern atmospheric conditions is a seemingly obvious initial choice, but it leads to low energy, overly smooth atmospheric properties (see, e.g., Zhai et al. 2012). A specific, arbitrarily chosen, year of modern atmospheric forcing is chosen as a more appropriate prior estimate. As was the case of the modern estimate of section 4, a daily mean of the 2006 NCEP–NCAR reanalysis product is used here.

The prior estimate of ocean conditions is based on OCCA, with modifications to provide a more LGM-like prior ocean state. Prior temperatures are reduced by 3°C everywhere, with minimum temperatures capped at −1.7°C, a value chosen to approximate the freezing point of seawater. Because of the lowered sea level, LGM mean ocean salinity was higher than the modern by about 1.1 (Adkins and Schrag 2001); pore fluid measurements also indicate that the ocean may have been significantly more salt stratified (Adkins et al. 2002). The prior salinity field used here is generated from OCCA by adding salt preferentially to deeper ocean layers in an approach that produces a mean salinity change of 1.1. Finally, monthly-mean conditions at all depths and longitudes of the 40°S southern boundary of the model are prescribed as follows: temperatures and salinities are modified from OCCA using the same approach as described for prior conditions, and the OCCA estimate of modern 40°S zonal and meridional velocities are used.

For comparison with observations, model estimates $\mathbf{E}(t)\mathbf{x}(t)$ are generated for each observation by identifying the model grid point closest to the given observation and then averaging the model conditions over an appropriate range of months [January–March (JFM) for the winter mean, July–September (JAS) for the summer mean, and over all 12 months for the annual mean] and over the top 30 m of the water column. The forward model simulation that results from the application of these assumptions, called LGM_Prior, is not consistent within error bars with the MARGO data, producing an initial misfit function $J_{\text{data}} = 10.7$. As shown in Fig. 4, the fit to MARGO is poor for all four proxy types and all seasons (winter, summer, and annual mean).

### b. Cost reduction

The cost function $J$ was then iteratively reduced from LGM_Prior; $J$ improved rapidly in early iterations, but as is common in nonlinear optimization, progress eventually slowed and then stalled after 51 iterations, at which point the cost function $J$ had been improved by 78%. Stalling can occur either because an acceptable solution has been reached or because of local numerical search difficulties. At iteration 51, $J_{\text{data}} = 1.1$, and that estimate (LGM_DR) was deemed satisfactory as a basis for analyzing the implied ocean state.

As compared to LGM_Prior, LGM_DR provides a much improved fit to all of the MARGO proxy types in all seasons (Fig. 4). Based on the summary statistics of Fig. 4, LGM_DR appears consistent with the data, with an important exception: the inconsistencies among the datasets have produced an estimate that compromises among them and which is thus systematically warmer or colder than the different types. Although not shown here, control variable adjustments are relatively modest in size, with nearly 100% of the adjustments smaller than the $\pm 2\sigma$ level (where $\sigma$ is the prior uncertainties given in Table 2).

### c. The LGM estimate

Inferred modern to LGM changes in annual-mean NSSTs (Fig. 5, left-hand plots) show moderate LGM cooling along the eastern boundary of the Atlantic Ocean, strong cooling in the eastern subpolar gyre south of Iceland, generally little change in the subtropical gyres, and a few degrees of LGM warming in the Gulf Stream region in winter. Patchiness in the estimated LGM_DR minus Mod_DR changes is likely an artifact of the data distribution (least squares solutions place unconstrained structures in data-sparse regions). Figure 6 shows the misfits between LGM_DR and MARGO. For the focus region between 25° and 5°W, LGM_DR is within the estimated uncertainty of most of the data. Significant misfits to the high-latitude alkenone and dinocyst data remain and are not fully accounted for by the data uncertainties (despite the doubled uncertainties).

#### 1) Dynamic topography and transports

Mean dynamic topography (MDT) is a useful representation of the long-term mean ocean circulation, as on the large scale, the circulation is very close to geostrophic balance. As shown in Fig. 7, the estimated LGM MDT is significantly different from the estimated modern, with increased transports in both the subpolar and subtropical gyres. A notable shift exists in the core of the subpolar gyre: while the modern subpolar gyre is most intense from south of Greenland into the Labrador Sea,

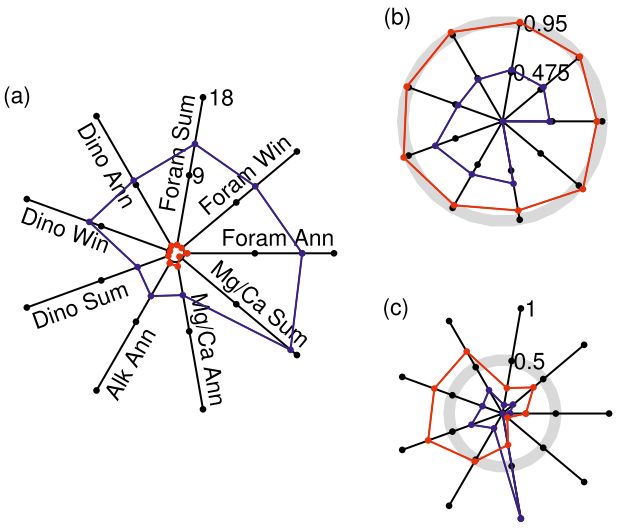


FIG. 4. Wheel diagrams showing model data misfit statistics for the posterior LGM_DR ocean state (red) as compared to those of the prior estimate (blue). Each radial line denotes a particular proxy type and season. Proxies include Mg/Ca, dinocyst and foraminifera assemblages (Dino and Foram), and alkenone-based temperatures (Alk); seasons include winter (Win), summer (Sum), and annual mean (Ann). (a) Radial distance shows $J_{\text{data}}$, where a radius of 1 is indicative of the consistency of the model with the data; a small circle is shown at a radius of 1. LGM_DR meets this condition. (b) The fraction of observational locations for which the model is within $\pm 2\sigma$ of the data is shown as radial distance. Consistency of model and data is indicated by fractions near 0.95, a condition met by LGM_DR. (c) Radial distance shows the fraction of observational locations for which the model is warmer than the data; values near 0.5 indicate minimal bias between the model and the data. LGM_DR shows less bias than the prior estimate but remains too cold (warm) compared to the dinocyst-based (foraminiferal assemblage based) NSST estimates.

the inferred LGM subpolar gyre is shifted significantly eastward, with the strongest transports extending from south of Greenland eastward to south of Iceland. A similar change was also inferred by Gebbie (2012). The front between the subpolar and subtropical gyres is more zonal in LGM_DR, such that the North Atlantic Current flows largely eastward toward Spain, rather than to the northeast, as in the modern ocean.

As suggested by the MDT, upper-ocean transports are increased in LGM_DR relative to today. Gulf Stream transport, defined as the integrated meridional transport at 29°N above 900 m and between 80° and 73.4°W, is 41 Sv (1 Sv $\equiv 10^6\,\text{m}^3\,\text{s}^{-1}$) of northward transport in LGM_DR, as compared to 35 Sv in OCCA. Likewise, the upper-ocean return flow, defined as the integrated meridional transport at 29°N above 900 m and east of 73.4°W, is 32 Sv southward in LGM_DR, as compared to 19 Sv in OCCA.

In the absence of transports to and from the Arctic, as assumed here, northward upper-ocean transport that is

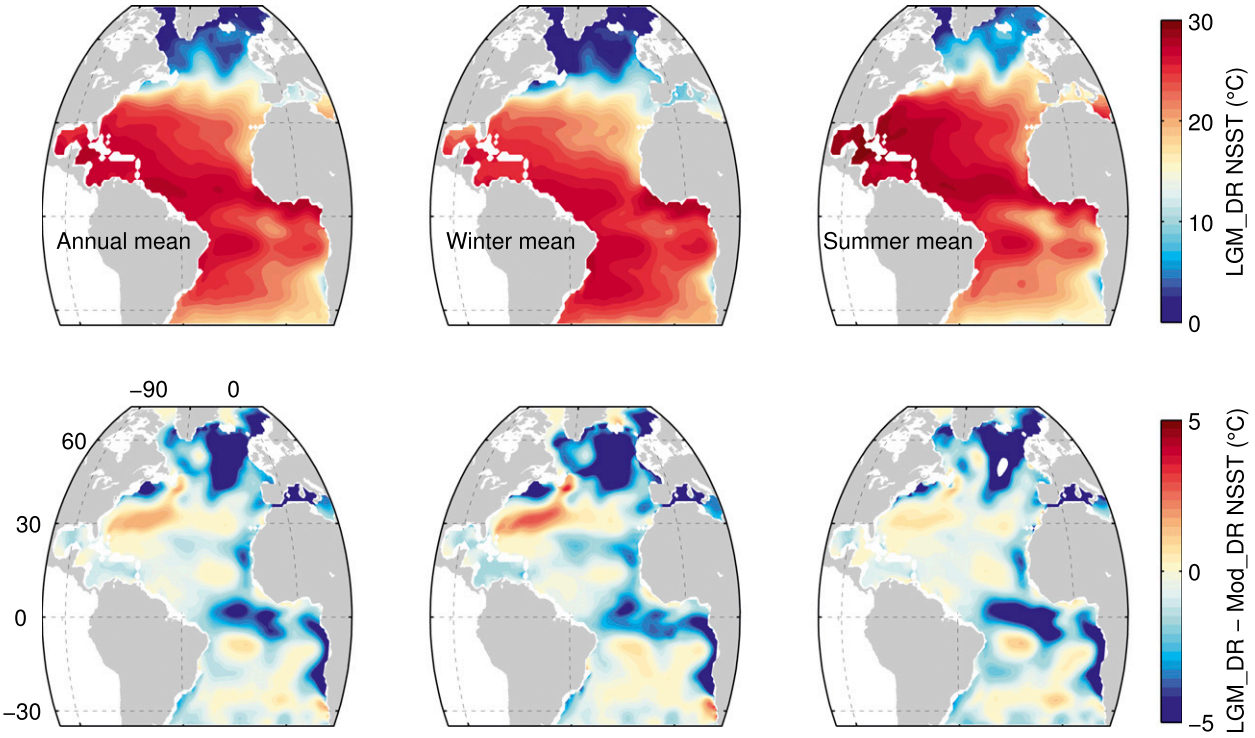


FIG. 5. (top) Annual-, winter-, and summer-mean NSST in LGM_DR and (bottom) difference from Mod_DR. Changes from LGM to modern are similar between (center) winter and (right) summer with a few exceptions: LGM equatorial cooling is particularly strong in summer, while LGM subpolar gyre cooling is more widespread in winter. Reconstructed NSSTs in the Gulf Stream region are warmer than modern in the LGM winter, but about the same as modern in the LGM summer (note that this is a region with sparse data coverage).

not compensated by an upper-ocean return flow must be compensated by a deep-ocean southward transport—the Atlantic meridional overturning circulation (AMOC). This inferred transport is 9 Sv in LGM_DR, as compared to 16 Sv in OCCA. There is sometimes a misconception that a weakened AMOC must be associated with weakened upper-ocean transports [see Wunsch and Heimbach (2013) for a discussion]. Here, although the inferred Gulf Stream transport is increased relative to today, the southward-flowing upper-ocean return flow is even more strongly increased. Therefore, even though both the northward- and southward-flowing upper-ocean transports are stronger than today, a weakened AMOC is inferred to exist. The LGM_DR AMOC is also substantially shallower than in OCCA, with most southward flow in LGM_DR occurring above 2500 m, while southward flows extend to 4500 m in OCCA. Estimated LGM deep-ocean conditions are preliminary at this time and will be discussed in a later paper.

The possibility of a more vigorous Atlantic circulation at the LGM has been proposed before (see, e.g., Curry and Oppo 2005). However, a number of other results have been taken to infer a reduced Atlantic circulation, most notably the results of Lynch-Stieglitz et al. (1999), who used $\delta^{18}O$ proxy observations to infer that Florida Straits' transport was about ⅔ of modern at the LGM. Two key uncertainties exist in the inference of a reduced Atlantic circulation based on these results. First, there is no information on a reference level velocity needed in applying the dynamic method to the LGM data in the Florida Straits (see Huybers and Wunsch 2010). Second, it is possible that a significant portion of the Gulf Stream transport traveled east of the Florida Straits at the LGM.

### 2) SEA ICE

As expected, inferred LGM sea ice extent is increased relative to today, particularly in winter (Fig. 8). Dinocyst and foraminifera assemblages can be used to reconstruct winter and summer sea ice extent, though uncertainties are larger than for NSST reconstruction (see, e.g., De Vernal et al. 2006). Both proxy approaches indicate very limited summer sea ice in the North Atlantic, as is also seen in LGM_DR. In winter, foraminiferal assemblage–based reconstructions indicate LGM sea ice presence along the east coast of Greenland and throughout the Labrador Sea, whereas dinocyst-based reconstructions indicate sparse LGM sea ice coverage except in the

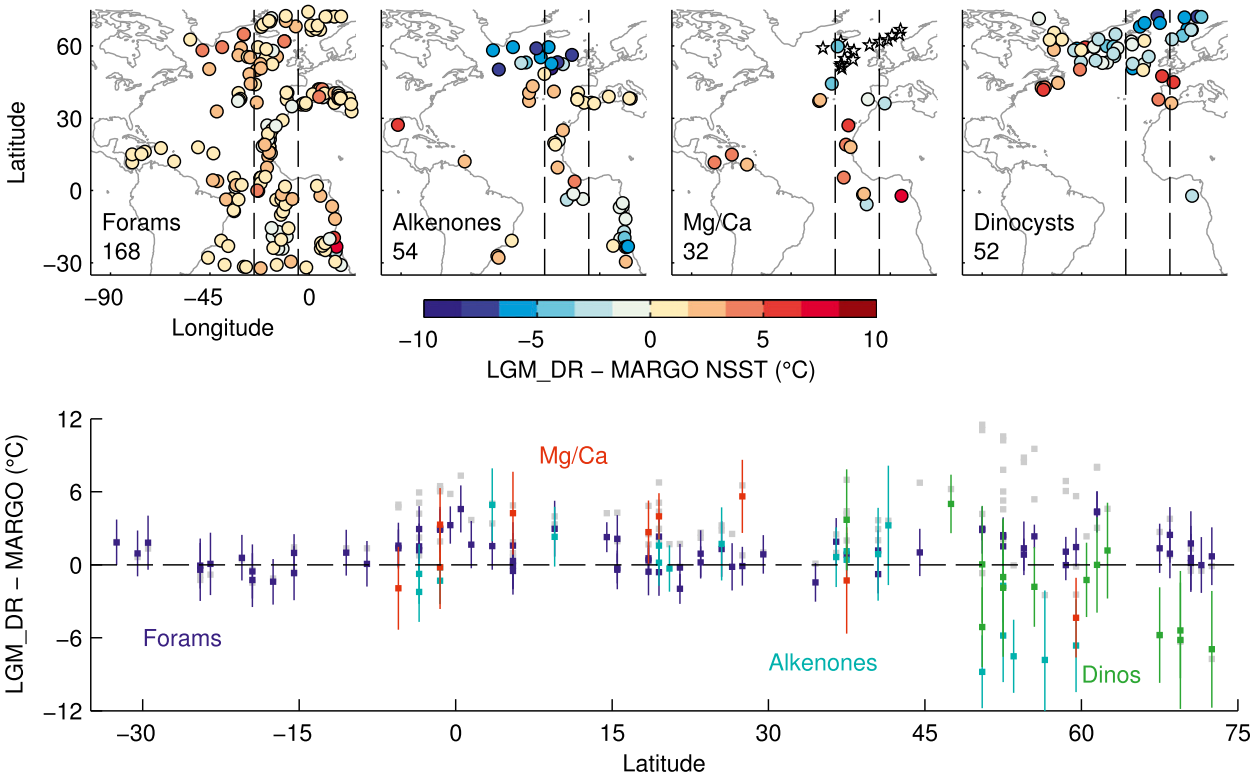


FIG. 6. As in Fig. 1, but showing misfits between annual-mean LGM NSST in LGM_DR and MARGO. (bottom) Data from 25° to 5°W are plotted against latitude, with Mod_DR − MARGO differences shown in gray for comparison. Uncertainties are modified from MARGO Project Members (2009) to double the uncertainties on alkenones north of 40°C and on dinocysts everywhere. LGM_DR is within uncertainty of most of the data.

Labrador Sea [see Dail (2012) for maps and discussion]. Winter sea ice cover in LGM_DR is in general agreement with the dinocyst-based reconstruction but does not agree with the foraminifera-based reconstruction. In a comparison with four PMIP2 LGM models, Dail (2012) found LGM_DR winter sea ice extent is similar to that simulated by the Model for Interdisciplinary Research on Climate, version 3.2 (MIROC3.2) and is significantly less extensive than that simulated by the Community Climate System Model, version 3 (CCSM3), Hadley Centre Coupled Model, version 3 (HadCM3), and Flexible Global Ocean–Atmosphere–Land System Model gridpoint, version 1.0 (FGOALS-g1.0). It is unclear which of the datasets or model results are most reliable. Sparse winter sea ice extent in LGM_DR may be related to the prior uncertainty assumptions made for the atmospheric control variables, which are both modest and spatially uniform (Table 2). Changes in sea ice cover are associated with changes in atmospheric forcing that are much larger than permitted by these prior uncertainties. For example, extreme changes in air temperature are observed when modern ocean conditions transition from ice free to ice covered.

### 3) ATMOSPHERIC CONDITIONS

The ocean property changes from the modern to the LGM described in the preceding paragraphs are produced by control adjustments in the model initial and southern boundary conditions and in the atmospheric forcing. Atmospheric conditions are the focus here, as they largely define the upper-ocean circulation in the 10-yr estimation periods used throughout this paper [see Dail (2012) for a discussion of all control adjustments]. Note that the approach used here does not include dynamical constraints on adjustments to atmospheric conditions; with significant improvements in technology, such constraints will become available through state estimation with coupled ocean–atmosphere models. In the current approach, the prior estimate of atmospheric forcing, which is a modern reanalysis, is assumed dynamically reasonable, and adjustments are constrained to be large scale and relatively modest in magnitude.

As seen in the top row of Fig. 9, LGM_DR shows large regions of increased annual-mean LGM wind speed with minimal regions of decreased wind speed. Upwelling-favorable winds are increased in the eastern equatorial

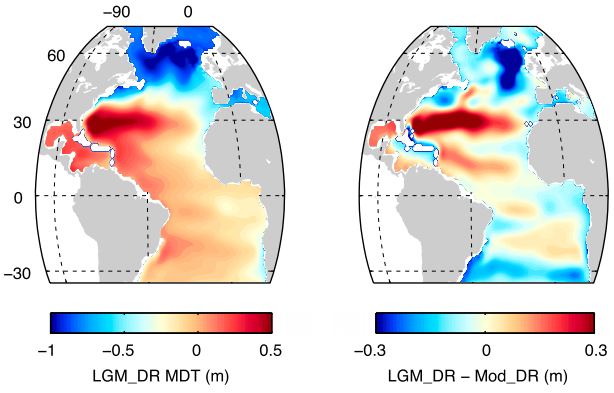


FIG. 7. (left) Mean dynamic topography in LGM_DR and (right) the difference from modern (LGM_DR − Mod_DR). The LGM reconstruction shows strengthened subtropical and subpolar gyre circulations and a more zonal subpolar front.

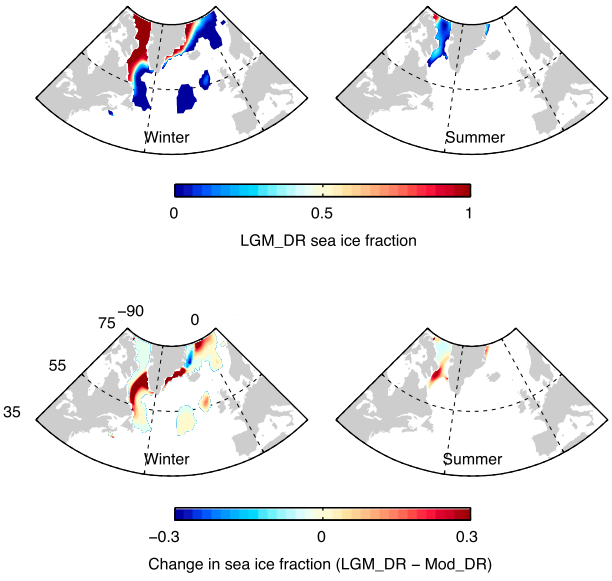


FIG. 8. (top) LGM_DR cell fraction covered by sea ice in winter (JFM) and summer (JAS) and (bottom) difference from Mod_DR. Inferred LGM sea ice is more extensive than in Mod_DR, especially in winter.

zone and in upwelling zones off the coast of Africa. An increase in strength of the Northern Hemisphere westerly and easterly winds implies an increased wind-driven circulation, consistent with the increases in midlatitude transports discussed above. Thermal wind balance under an increased equator to pole temperature gradient would seem to suggest such a response; Li and Battisti (2008) note such an increase in the mean westerly wind strength in the Atlantic in the CCSM3 PMIP2 LGM simulation.

Annual-mean LGM_DR air temperatures (Fig. 9, middle row) show intense cooling of 3°–5°C in the eastern low latitudes and over 5°C in the subpolar gyre; elsewhere, differences between modern and inferred LGM air temperatures are smaller than 1°–2°C. Although the magnitude of air temperature change seen here is similar to that of the PMIP2 ensemble mean (Braconnot et al. 2007), PMIP2 models vary significantly in the regional pattern of cooling.

Given the lack of reliable LGM salinity data, evaporation and precipitation are poorly constrained. Nonetheless, their rates are affected by the control adjustments and influence the ocean circulation through salinity changes. Figure 9 (top right) shows that, like the modern Atlantic, LGM_DR has net evaporation in the subtropical gyres and net freshwater input near the Amazon and in the subpolar gyre. LGM-modern differences (Fig. 9, bottom right) show less LGM freshwater flux into the ocean (drier conditions) across much of the Atlantic, with wetter LGM conditions north of 60°N, in the western Northern Hemisphere subtropical gyre, and in the western equatorial zone. See Boos (2012) for a discussion of the LGM hydrological cycle in PMIP2 models.

#### 4) SEASONALITY

LGM_DR shows similar seasonality to Mod_DR, with differences that are small scale, noisy, and a few degrees Celsius in amplitude (Fig. 10). As mentioned previously, the change in sea ice extent between LGM_DR and Mod_DR is larger in winter than in summer (Fig. 8). The largest affected region is the region south of Greenland, which does show increased NSST seasonality in LGM_DR in Fig. 10. Sea ice is highly sensitive to temperature changes in cold regions that are close to the freezing point, so that relatively small changes in NSST can have a substantial impact on sea ice extent.

### *d. Sensitivity to uncertainty assumptions*

A series of assumptions has been made in forming the LGM_DR estimate of the upper-ocean circulation and its forcing. These assumptions include that the model is adequate to depict the major physical elements of the ocean circulation; the data are consistent with a fixed seasonal cycle; modern meteorology is a useful (but not limiting) starting estimate; and estimated errors in the proxy data are realistic. Much could be learned by testing these and other assumptions in sensitivity studies, but testing all assumptions is not practical. As important special cases, the sensitivity of the dynamical reconstruction to uncertainty assumptions on the MARGO data, and on the wind speed components of the atmospheric forcing, is now examined.

Two alternative data uncertainty assumptions are tested here. LGM_S1 (for LGM sensitivity study 1) is a dynamical reconstruction that uses all of the same assumptions as our reference solution, LGM_DR, except that the published MARGO uncertainties are used

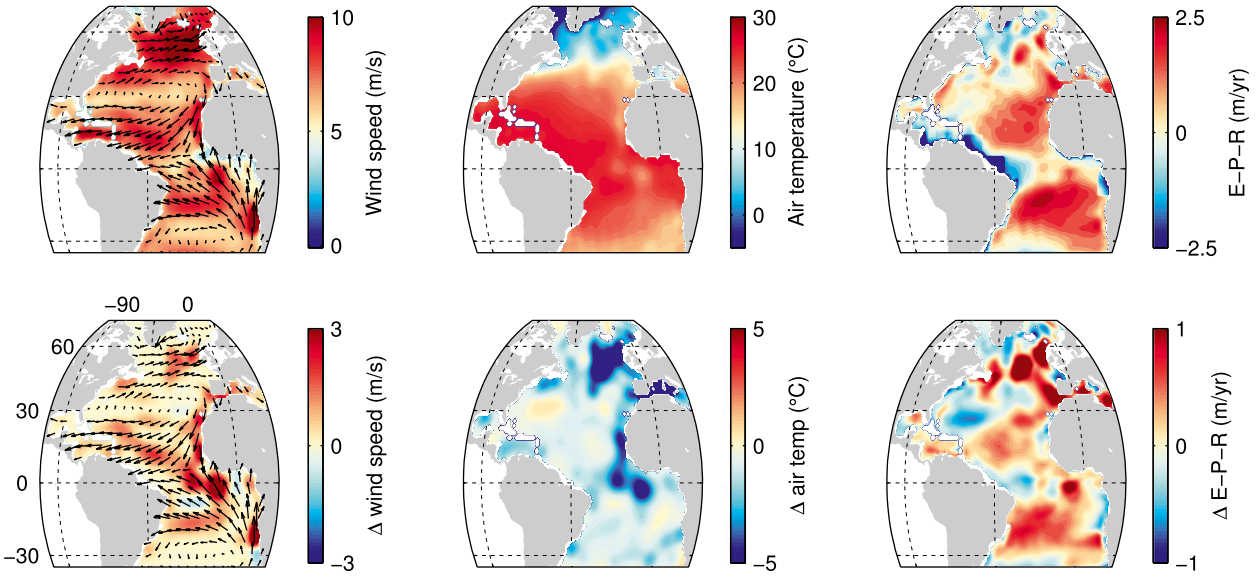


FIG. 9. (top) Annual-mean adjusted atmospheric forcing for LGM_DR and (bottom) LGM_DR − NCEP differences. (left) Wind speed and wind speed anomaly are shown in colors; vectors in both plots show the LGM_DR wind direction. (center) Air temperature and LGM-modern differences. (right) Net freshwater flux (evaporation–precipitation–runoff), where positive values in the top panel indicate net evaporation and positive values in the bottom panel indicate that the inferred LGM climate is drier than modern.

without modification. As expected from previous discussions of the high-latitude mismatches between datasets, LGM_S1 cannot provide an adequate mean fit to the data (Fig. 11). In keeping with the stronger emphasis in LGM_S1 on the high-latitude dinocyst and alkenone data, high-latitude NSSTs are warmer in LGM_S1 than in LGM_DR (Fig. 12). For the second test, LGM_S2, all dinocyst, Mg/Ca, and alkenone uncertainties are assumed infinite (i.e., these data are excluded). Fitting the remaining foraminiferal assemblage–based data is then easier than it was in LGM_DR (Fig. 11). North of 50°N, LGM_S2 is colder than LGM_DR (Fig. 12), just as the foraminiferal assemblage–based NSST data are colder than those of the dinocyst and alkenone data at these latitudes.

Because the ocean circulation is highly sensitive to the applied wind stress (computed in this model from wind velocity), we consider how sensitive the dynamical reconstruction is to the uncertainties assumed for the prior wind speed. LGM_S3 uses all of the same data, data uncertainties, and other assumptions as LGM_DR, with the exception of the wind speed uncertainty, which is $1\,\mathrm{m\,s^{-1}}$ in LGM_S3 as compared to $2\,\mathrm{m\,s^{-1}}$ in LGM_DR. Likewise, LGM_S4 uses an uncertainty of $4\,\mathrm{m\,s^{-1}}$. As might be expected, as larger control adjustments are permitted, the dynamical reconstruction approach is able to provide a better fit to the data (Fig. 13). Patterns of wind speed adjustment for LGM_S3 and LGM_S4 are similar to those shown in Fig. 9 for LGM_DR, though the magnitude of the adjustments grows with the assigned uncertainty. Likewise, as the uncertainty in the wind speed components is increased, inferred upper-ocean transports are increased. For example, Gulf Stream transport increases from 32 Sv for LGM_S3 to 41 Sv for LGM_DR and to 44 Sv for LGM_S4. Thus, the trade-off for a better fit to the ocean data is inferred LGM wind speeds that are more extreme, as compared to modern conditions.

As expected, dynamical reconstructions are sensitive to the uncertainties assigned to the data and the control variables. Although LGM_DR is our best estimate, other reasonable assumptions also lead to potentially acceptable results. In comparison with the experience in making similar estimates of the modern ocean circulation (Wunsch and Heimbach 2013), the major issue is the sparse database. Although better models, particularly with higher resolution and global extent, can likely make improved estimates compared to those described here, without far more data determining the meteorological conditions and the internal oceanic state, such estimates will continue to have large uncertainties.

## 6. Discussion

A dynamical reconstruction (state estimate) of the LGM Atlantic Ocean has been obtained. The estimate is based on the MARGO near–sea surface temperature proxy records, a full general circulation and sea ice model, uncertainties in the data, and uncertainties in the prior estimates of the model atmospheric forcing and initial conditions. As with studies of the modern

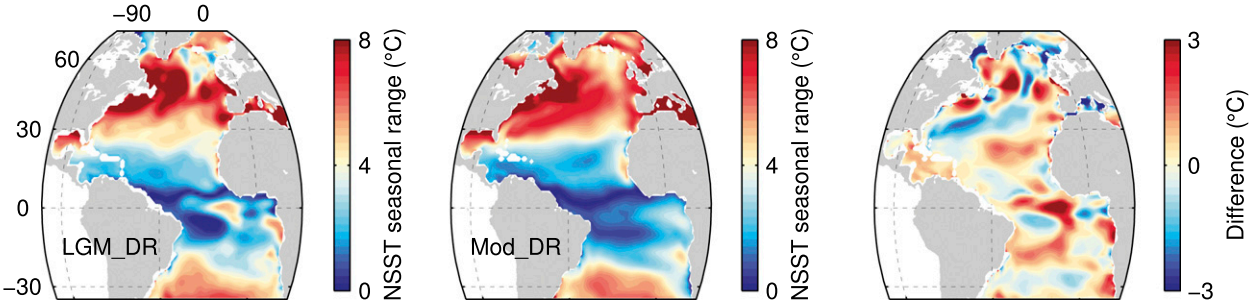


FIG. 10. Seasonal range (|summer − winter|) in NSST for (left) LGM_DR, (center) Mod_DR, and the (right) difference in seasonal range (LGM_DR − Mod_DR). Red colors in the right-hand map indicate regions where LGM_DR has a larger seasonal range in NSST than Mod_DR. Inferred changes in seasonality are small scale and noisy—large, basin-scale changes in seasonality between the LGM and today are not indicated by the approach used here.

circulation, numerical solution of the constrained least squares problem using Lagrange multipliers proves to be useful in practice. The resulting solution, including estimates of the meteorological forcing, contrasts with published LGM forward modeling efforts, which have not succeeded in providing a close fit to proxy estimates of LGM NSSTs. As in any estimation problem, no claim is made that LGM_DR is correct—only that it exactly satisfies known adjusted model equations and is generally consistent with the observations insofar as that is possible.

Disagreements among the four MARGO NSST compilations used here are sometimes large, especially north of 40°N, and the uncertainty assignments suggested as a first estimate on site-specific proxies in MARGO Project Members (2009) are insufficient to permit reconciliation of these datasets. However, if uncertainties are doubled on dinocyst data everywhere and on alkenone data north of 40°N, it is possible to identify an ocean state, LGM_DR, that agrees relatively well with MARGO NSST estimates. Previously, it was unknown how closely a numerical model could reproduce observed LGM NSSTs.

An important inference is that moderate changes from the modern atmosphere are sufficient to reproduce LGM NSSTs—wholesale reorganizations are not required. As compared to the modern atmosphere, required changes include increases in the strength of easterly and westerly winds, increases in upwelling favorable winds in the eastern equatorial zone and along the western African coast, 4°C or more of cooling of air temperatures in the eastern subpolar gyre and eastern equatorial zone, and large-scale increases in net surface freshwater flux out of the Atlantic. LGM_DR is also marked by several key differences from the modern ocean state: strong decreases in NSST in the eastern equatorial Atlantic and eastern subpolar gyre, a significant eastward shift of the core of the subpolar gyre, increased upper-ocean transports in the subpolar and subtropical gyres, increased zonality of the North Atlantic current, and increased sea ice extent, especially in winter. These inferred changes are a baseline solution for further study, and we note that much larger differences might have existed—only that they do not appear to be required by the model physics or the MARGO NSST data.

A number of limitations of the current study are important. Among them are the assumptions that, to first order, the LGM Atlantic Ocean can be represented with a fixed seasonal cycle and that interannual variability can be neglected. Longer-term variability is surely present, but the database used does not depict it. A 10-yr state estimate has been used here under the assumption that

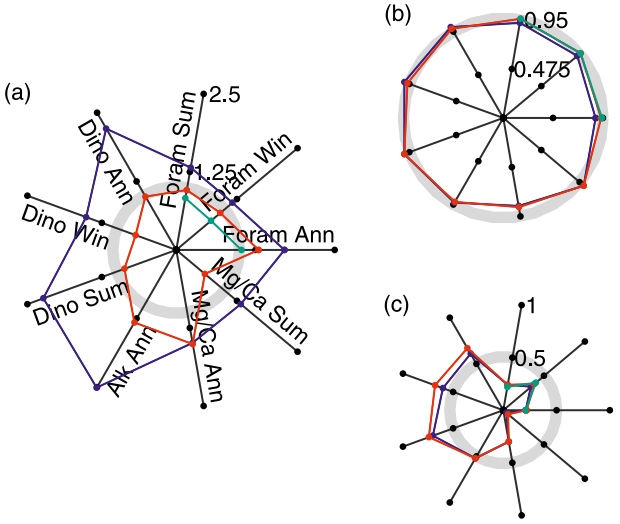


FIG. 11. Prior uncertainty assumptions on the data impact the estimate and its fit to the various MARGO datasets. As in Fig. 4, but employs a gray, rather than black, circle to mark a radius of 1. LGM_S1, which uses published MARGO uncertainties, is shown in blue; LGM_DR is shown in red; and LGM_S2, which excludes the dinocyst, Mg/Ca and alkenone data altogether, is shown in green. (a) Using smaller uncertainties, as in LGM_S1, makes fitting the data more difficult, whereas excluding some datasets, as in LGM_S2, makes fitting the remaining data easier. Differences between the three estimates in (b) and (c) are relatively small.

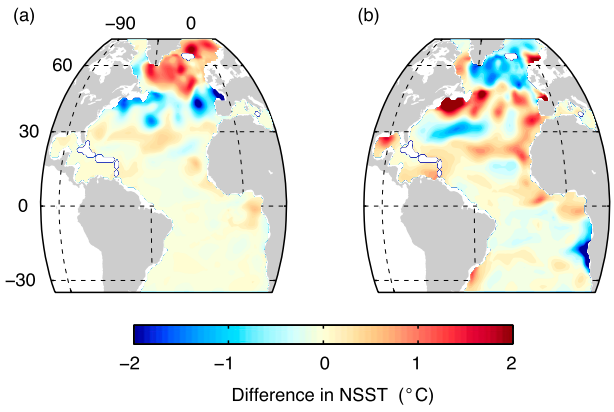


FIG. 12. (left) Difference between annual-mean NSST in LGM_S1, which uses published MARGO uncertainties, and LGM_DR, which uses uncertainties twice as large on alkenones north of 40°N and on dinocysts everywhere. The increased influence of the alkenone and dinocyst data in LGM_S1 leads to warmer NSSTs north of about 45°N and cooler temperatures from 30° to 45°N. (right) Difference between LGM_S2, which excludes all dinocyst, Mg/Ca, and alkenone data and LGM_DR. North of 30°N the pattern is nearly the opposite of that in the left-hand panel. The mostly positive anomalies south of 30°N indicate that the foraminiferal assemblage–based data is overall slightly warmer at these latitudes than the other three datasets.

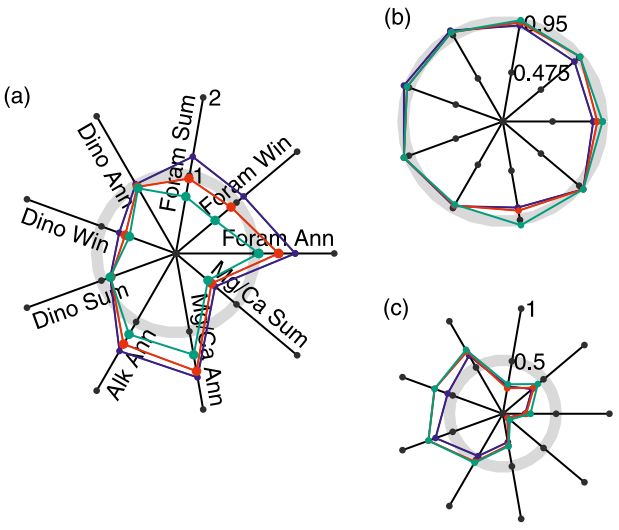


FIG. 13. Prior uncertainty assumptions on wind speed control variables impact the extent to which the reconstruction approach can fit the data. As in Fig. 4, but employs a gray, rather than black, circle to mark a radius of 1. Uncertainties on the wind speed control variable components are increased from 1 m s$^{-1}$ in LGM_S3 (blue) to 2 m s$^{-1}$ in LGM_DR (red) and to 4 m s$^{-1}$ in LGM_S4 (green). (a) The fit to the data is improved as larger control variable adjustments are permitted. Differences between the three estimates in (b) and (c) are relatively small.

upper-ocean conditions are largely controlled by atmospheric forcing and that the upper-ocean properties are reasonably close to equilibrium with atmospheric forcing after that time. This assumption can be tested by studying the sensitivity of estimated conditions to state estimate duration and to the choice of initial conditions in the ocean.

Modern atmospheric conditions have been used here as an a priori estimate of atmospheric forcing. In principle, the dynamical reconstruction approach can be applied to a coupled ocean–atmosphere–sea ice model, although such approaches, for technical reasons, have not yet been rendered practical even in the modern world. Meteorological fields from coupled model simulations of the LGM could be used as priors to evaluate the sensitivity of the estimated conditions to these choices. More generally, uncertainty quantification for both ordinary models as well as adjoint-based state estimates is needed but has been problematic for technical reasons. Recent progress in this area on simplified problems is encouraging (Kalmikov 2013), although it is not yet applicable to full problems such as the current one.

The distribution of LGM NSST data is sparse and uneven, and the proxies show substantial disagreements with each other. Known key aspects of the ocean state, such as salinity, are largely unconstrained by available LGM data. Continued proxy development is key to improving future state estimates, even as more elaborate models could be used.

A first step has been taken down the road toward a critical objective—the ability to find dynamically consistent estimates of the glacial ocean that are also consistent with diverse proxy records. Discussions will be published elsewhere of the implied full water column circulation. We anticipate that this approach will prove useful in a variety of studies, including the use of a higher-resolution global model, the inclusion of additional oceanic data types, the consideration of data constraints on paleoatmospheric properties, and application of the method for defining future sampling strategies.

*Acknowledgments.* Olivier Marchal, Jake Gebbie, and Claire Waelbroeck provided helpful reviews on an earlier version of this manuscript; suggestions from three anonymous reviewers also improved the manuscript. Gaël Forget, Matt Mazloff, Patrick Heimbach, and Jean-Michel Campin provided much appreciated technical assistance with state estimation. The work of the MARGO Project participants, and those who collected the records compiled in MARGO, make studies such as this one possible. We also thank the participants of the PMIP project for making their simulation results available. NASA and NCAR computational resources were used for all simulations reported in this study. This work was funded by a National Defense Science and Engineering Graduate Fellowship and National Science Foundation Awards OCE-0645936 and OCE-1060735.

## REFERENCES


Adcroft, A. J., C. N. Hill, and J. C. Marshall, 1999: A new treatment of the Coriolis terms in C-grid models at both high and low resolutions. *Mon. Wea. Rev.,* **127,** 1928–1936.

——, ——, J. Campin, J. Marshall, and P. Heimbach, 2004: Overview of the formulation and numerics of the MIT GCM. *Proc. ECMWF Seminar Series on Numerical Methods, Recent Developments in Numerical Methods for Atmosphere and Ocean Modelling,* Shinfield Park, United Kingdom, ECMWF, 139–149.

Adkins, J. F., and D. P. Schrag, 2001: Pore fluid constraints on deep ocean temperature and salinity during the Last Glacial Maximum. *Geophys. Res. Lett.,* **28,** 771–774.

——, K. McIntyre, and D. Schrag, 2002: The salinity, temperature, and $\delta^{18}O$ of the glacial deep ocean. *Science,* **298,** 1769–1773.

Arakawa, A., and V. Lamb, 1977: Computational design of the basic dynamical processes of the UCLA general circulation model. *Methods Comput. Phys.,* **17,** 174–267.

Barker, S., I. Cacho, H. Benway, and K. Tachikawa, 2005: Planktonic foraminiferal Mg/Ca as a proxy for past oceanic temperatures: A methodological overview and data compilation for the Last Glacial Maximum. *Quat. Sci. Rev.,* **24,** 821–834.

Barnola, J., D. Raynaud, Y. Korotkevich, and C. Lorius, 1987: Vostok ice core provides 160,000-year record of atmospheric $CO_2$. *Nature,* **329,** 408–414.

Boos, W., 2012: Thermodynamic scaling of the hydrological cycle of the Last Glacial Maximum. *J. Climate,* **25,** 992–1006.

Braconnot, P., and Coauthors, 2007: Results of PMIP2 coupled simulations of the mid-Holocene and Last Glacial Maximum—Part 1: Experiments and large-scale features. *Climate Past,* **3,** 261–277.

——, S. P. Harrison, M. Kageyama, P. J. Bartlein, V. Masson-Delmotte, A. Abe-Ouchi, B. Otto-Bliesner, and Y. Zhao, 2012: Evaluation of climate models using palaeoclimatic data. *Nat. Climate Change,* **2,** 417–424.

Burke, A., O. Marchal, L. I. Bradtmiller, J. F. Mcmanus, and R. Francois, 2011: Application of an inverse method to interpret $^{231}Pa/^{230}Th$ observations from marine sediments. *Paleoceanography,* **26,** PA1212, doi:10.1029/2010PA002022.

CLIMAP Project Members, 1976: The surface of the ice-age Earth. *Science,* **191,** 1131–1137.

Conte, M., M.-A. Sicre, C. Rühlemann, J. Weber, S. Schulte, D. Schulz-Bull, and T. Blanz, 2006: Global temperature calibration of the alkenone unsaturation index ($U^{K'}_{37}$) in surface waters and comparison with surface sediments. *Geochem. Geophys. Geosyst.,* **7,** Q02005, doi:10.1029/2005GC001054.

Curry, W. B., and D. W. Oppo, 2005: Glacial water mass geometry and the distribution of $\delta^{13}C$ of $\Sigma CO_2$ in the western Atlantic Ocean. *Paleoceanography,* **20,** PA1017, doi:10.1029/2004PA001021.

Dail, H., 2012: Atlantic Ocean circulation at the Last Glacial Maximum: Inferences from data and models. Ph.D. dissertation, MIT/WHOI Joint Program, 236 pp. [Available online at http://hdl.handle.net/1721.1/78367.]

Dale, B., 2001: The sedimentary record of dinoflagellate cysts: Looking back into the future of phytoplankton blooms. *Sci. Mar.,* **65,** 257–272.

De Vernal, A., and Coauthors, 2005: Reconstruction of sea-surface conditions at middle to high latitudes of the Northern Hemisphere during the Last Glacial Maximum (LGM) based on dinoflagellate cyst assemblages. *Quat. Sci. Rev.,* **24,** 897–924.

——, A. Rosell-Melé, M. Kucera, C. Hillaire-Marcel, F. Eynaud, M. Weinelt, T. Dokken, and M. Kageyama, 2006: Comparing proxies for the reconstruction of LGM sea-surface conditions in the northern North Atlantic. *Quat. Sci. Rev.,* **25,** 2820–2834.

Forget, G., 2010: Mapping ocean observations in a dynamical framework: A 2004–06 ocean atlas. *J. Phys. Oceanogr.,* **40,** 1201–1221.

——, and C. Wunsch, 2007: Estimated global hydrographic variability. *J. Phys. Oceanogr.,* **37,** 1997–2008.

Gaspar, P., Y. Gregoris, and J. M. Lefevre, 1990: A simple eddy kinetic energy model for simulations of the oceanic vertical mixing: Tests at station Papa and long-term upper ocean study site. *J. Geophys. Res.,* **95** (C9), 179–192.

Gebbie, G., 2012: Tracer transport timescales and the observed Atlantic-Pacific lag in the timing of the last termination. *Paleoceanography,* **27,** PA3225, doi:10.1029/2011PA002273.

——, and P. Huybers, 2006: Meridional circulation during the Last Glacial Maximum explored through a combination of South Atlantic $\delta^{18}O$ observations and a geostrophic inverse model. *Geochem. Geophys. Geosyst.,* **7,** Q11N07, doi:10.1029/2006GC001383.

Gent, P., and J. McWilliams, 1990: Isopycnal mixing in ocean circulation models. *J. Phys. Oceanogr.,* **20,** 150–155.

Giering, R., and T. Kaminski, 1998: Recipes for adjoint code construction. *ACM Trans. Math. Software,* **24,** 437–474.

Hargreaves, J., A. Paul, R. Ohgaito, A. Abe-Ouchi, and J. D. Annan, 2011: Are paleoclimate model ensembles consistent with the MARGO data synthesis? *Climate Past,* **7,** 917–933.

Hayes, A., M. Kucera, N. Kallel, L. Sbaffi, and E. Rohling, 2005: Glacial Mediterranean sea surface temperatures based on planktonic foraminiferal assemblages. *Quat. Sci. Rev.,* **24,** 999–1016.

Heimbach, P., C. Hill, and R. Giering, 2005: An efficient exact adjoint of the parallel MIT general circulation model, generated via automatic differentiation. *Future Gener. Comput. Syst.,* **21,** 1356–1371.

Henderson, G., 2002: New oceanic proxies for paleoclimate. *Earth Planet. Sci. Lett.,* **203,** 1–13.

Hillaire-Marcel, C., and A. De Vernal, Eds., 2007: *Proxies in Late Cenozoic Paleoceanography.* Developments in Marine Geology Series, Vol. 1, Elsevier, 862 pp.

Huybers, P., and C. Wunsch, 2010: Paleophysical oceanography with an emphasis on transport rates. *Annu. Rev. Mar. Sci.,* **2,** 1–34.

Kageyama, M., A. Laīné, and A. Abe-Ouchi, 2006: Last Glacial Maximum temperatures over the North Atlantic, Europe and western Siberia: A comparison between PMIP models, MARGO sea-surface temperatures and pollen-based reconstructions. *Quat. Sci. Rev.,* **25,** 2082–2102.

Kalmikov, A., 2013: Uncertainty quantification in ocean state estimation. Ph.D. dissertation, MIT/WHOI Joint Program, 160 pp. [Available online at http://hdl.handle.net/1721.1/79291.]

Kalnay, E., and Coauthors, 1996: The NCEP/NCAR 40-Year Reanalysis Project. *Bull. Amer. Meteor. Soc.,* **77,** 437–471.

Kucera, M., A. Rosell-Melé, R. Schneider, C. Waelbroeck, and M. Weinelt, 2005a: Multiproxy Approach for the Reconstruction of the Glacial Ocean Surface (MARGO). *Quat. Sci. Rev.,* **24,** 813–819.

——, and Coauthors, 2005b: Reconstruction of sea-surface temperatures from assemblages of planktonic foraminifera: Multi-technique approach based on geographically constrained calibration data sets and its application to glacial Atlantic and Pacific Oceans. *Quat. Sci. Rev.,* **24,** 951–998.

Lambeck, K., and J. Chappell, 2001: Sea level change through the last glacial cycle. *Science,* **292,** 679–686.

Large, W., and S. Yeager, 2004: Diurnal to decadal global forcing for ocean and sea-ice models: The data sets and flux climatologies. Tech. Rep. NCAR TN-4601STR, 112 pp.

——, J. McWilliams, and S. Doney, 1994: Oceanic vertical mixing: A review and a model with a non-local k-profile boundary layer parameterization. *Rev. Geophys.,* **32,** 363–403.

Leduc, G., R. Schneider, J.-H. Kim, and G. Lohmann, 2010: Holocene and Eemian sea surface temperature trends as revealed by alkenone and Mg/Ca paleothermometry. *Quat. Sci. Rev.,* **29,** 989–1004.

LeGrand, P., and C. Wunsch, 1995: Constraints from paleotracer data on the North Atlantic circulation during the Last Glacial Maximum. *Paleoceanography,* **10,** 1011–1045.

Li, C., and D. S. Battisti, 2008: Reduced Atlantic storminess during Last Glacial Maximum: Evidence from a coupled climate model. *J. Climate,* **21,** 3561–3579.

Losch, M., D. Menemenlis, J. M. Campin, P. Heimbach, and C. Hill, 2010: On the formulation of sea-ice models. Part 1: Effects of different solver implementations and parameterizations. *Ocean Modell.,* **33,** 129–144.

Lynch-Stieglitz, J., 2003: Tracers of past ocean circulation. *Treatise on Geochemistry,* Vol. 6, H. Elderfield, Ed., Elsevier, 433–451.

——, W. B. Curry, and N. Slowey, 1999: Weaker Gulf Stream in the Florida straits during the Last Glacial Maximum. *Nature,* **402,** 644–648.

Marchal, O., and W. B. Curry, 2008: On the abyssal circulation in the glacial Atlantic. *J. Phys. Oceanogr.,* **38,** 2014–2037.

MARGO Project Members, 2009: Constraints on the magnitude and patterns of ocean cooling at the Last Glacial Maximum. *Nat. Geosci.,* **2,** 127–132.

Marshall, J., A. Adcroft, C. Hill, L. Perelman, and C. Heisey, 1997: A finite-volume, incompressible Navier Stokes model for studies of the ocean on parallel computers. *J. Geophys. Res.,* **102** (C3), 5753–5766.

Otto-Bliesner, B. L., C. Hewitt, T. M. Marchitto, E. C. Brady, A. Abe-Ouchi, M. Crucifix, S. Murakami, and S. L. Weber, 2007: Last Glacial Maximum ocean thermohaline circulation: PMIP2 model intercomparisons and data constraints. *Geophys. Res. Lett.,* **34,** L12706, doi:10.1029/2007GL029475.

——, and Coauthors, 2009: A comparison of PMIP2 model simulations and the MARGO proxy reconstruction for tropical sea surface temperatures at Last Glacial Maximum. *Climate Dyn.,* **32,** 799–815.

Peltier, W. R., 2004: Global glacial isostasy and the surface of the ice-age Earth: The ICE-5G (VM2) model and GRACE. *Annu. Rev. Earth Planet. Sci.,* **32,** 111–149.

Redi, M., 1982: Oceanic isopycnal mixing by coordinate rotation. *J. Phys. Oceanogr.,* **12,** 1154–1158.

Rosell-Melé, A., E. Bard, K.-C. Emeis, B. Grieger, C. Hewitt, P. Müller, and R. Schneider, 2004: Sea surface temperature anomalies in the oceans at the LGM estimated from the alkenone-$U_{37}^{K'}$ index: Comparison with GCMs. *Geophys. Res. Lett.,* **31,** L03208, doi:10.1029/2003GL018151.

Sarnthein, M., R. Gersonde, S. Niebler, U. Pflaumann, R. Spielhagen, J. Thiede, G. Wefer, and M. Weinelt, 2003: Overview of Glacial Atlantic Ocean Mapping (GLAMAP 2000). *Paleoceanography,* **18,** 1030, doi:10.1029/2002PA000769.

Schneider, B., G. Leduc, and W. Park, 2010: Disentangling seasonal signals in Holocene climate trends by satellite-model-proxy integration. *Paleoceanography,* **25,** PA4217, doi:10.1029/2009PA001893.

Stammer, D., and Coauthors, 2002: Global ocean circulation during 1992–1997, estimated from ocean observations and a general circulation model. *J. Geophys. Res.,* **107,** 3118, doi:10.1029/2001JC000888.

Telford, R., C. Li, and M. Kucera, 2013: Mismatch between the depth habitat of planktonic foraminifera and the calibration depth of SST transfer functions may bias reconstructions. *Climate Past,* **9,** 859–870.

Waelbroeck, C., S. Mulitza, H. Spero, T. Dokken, T. Kiefer, and E. Cortijo, 2005: A global compilation of late Holocene planktonic foraminiferal $\delta^{18}O$: Relationship between surface water temperature and $\delta^{18}O$. *Quat. Sci. Rev.,* **24,** 853–868.

Weaver, A., and P. Courtier, 2001: Correlation modelling on the sphere using a generalized diffusion equation. *Quart. J. Roy. Meteor. Soc.,* **127,** 1815–1846.

Winguth, A., D. Archer, J.-C. Duplessy, E. Maier-Reimer, and U. Mikolajewicz, 1999: Sensitivity of paleonutrient tracer distributions and deep-sea circulation to glacial boundary conditions. *Paleoceanography,* **14,** 304–323.

Wunsch, C., 2006: *Discrete Inverse and State Estimation Problems: With Geophysical Fluid Applications.* Cambridge University Press, 384 pp.

——, and P. Heimbach, 2007: Practical global oceanic state estimation. *Physica D,* **230,** 197–208.

——, and ——, 2013: Dynamically and kinematically consistent global ocean circulation state estimates with land and sea ice. *Ocean Circulation and Climate: A 21st Century Perspective,* 2nd ed. G. Siedler et al., Eds., International Geophysics, Vol. 103, Academic Press, 553–579.

——, ——, R. Ponte, and I. Fukumori, 2009: The global general circulation of the ocean estimated by the ECCO-Consortium. *Oceanography,* **22,** 88–103.

Zhai, X., H. Johnson, D. Marshall, and C. Wunsch, 2012: On the wind power input to the ocean general circulation. *J. Phys. Oceanogr.,* **42,** 1357–1365.